Anomalous stopping of laser-accelerated intense proton beam in dense ionized matter

Jieru Ren,[1] Zhigang Deng,[2] Benzheng Chen,[1] Dong Wu,[3,*] Bubo Ma,[1] Xing Wang,[1] Shuai Yin,[1] Jianhua Feng,[1] Wei Liu,[1] Dieter Hoffmann,[1] Wei Qi,[2] Shaoyi Wang,[2] Quanping Fan,[2] Bo Cui,[2] Zongqing Zhao,[2] Leifeng Cao,[2] Shaoping Zhu,[2] Rui Cheng,[4] Xianming Zhou,[4] Yihang Zhang,[5] Zhe Zhang,[5] Yutong Li,[5] Weimin Zhou,[2,†] and Yongtao Zhao[1,‡]

[1] *School of Science, Xi'an Jiaotong University, Xi'an 710049, China*
[2] *Laser Fusion Research Center, Chinese Academy of Engineering Physics, Mianyang*
[3] *Institute for Fusion Theory and Simulation, Department of Physics, Zhejiang University, Hangzhou, 310058, China*
[4] *Institute of Modern Physics, Chinese Academy of Sciences, Lanzhou, 710049, China*
[5] *Institute of Physics, Chinese Academy of Sciences, Beijing, 100190, China*

(Dated: September 26, 2019)

We report first experimental evidence on anomalous stopping and significantly enhanced stopping power of dense ionized matter interacting with a high-current laser-generated proton beam. A magnetic dipole was used to tailor a short and quasi-mono-energetic proton beam of 3.4 MeV with an energy spread of 6%. The target of dense ionized matter was produced from irradiating a carbon-hydrogen-oxygen foam sample (TAC) with soft x-rays from a laser-heated hohlraum. The hydrodynamic timescale of the target is long compared to the short proton beam pulse and therefore the target can be considered to be quasi static with well characterized plasma parameters of 17 eV electron temperature and an electron number density of 4×10^{20} cm^{-3}. We observed enhanced stopping properties by one order of magnitude as compared to the classical single particle stopping in cold matter. We attribute this phenomenon to a strong decelerating electric field with a maximum on the order of 10^9 V/m, which is induced by the intense proton beam. Our numerical simulation shows that this collective effect plays the dominant role, and it will have major impact on nuclear fusion scenarios like fast ignition, but also for applications in material science and astrophysics.

Ion beam stopping in ionized matter is a fundamental process of utmost importance to nuclear fusion. In fusion plasmas, we have to deal with alpha particle stopping with the constituents of fully ionized Deuterium-Tritium plasma, where binary collisions prevail and no collective phenomena are predicted or observed. Even in the case of ion driven fusion, which requires the highest beam intensity from accelerators [1] no collective effects on ion stopping processes due to high beam intensity are considered nor–to the best of our knowledge–were they reported in any high current experiment. The situation is quite different for the fast ignition scheme (FI), proposed independently by N. G. Basov [2] and later M. Tabak [3]. Here a short and intense pulse of high energy charged particles–electrons, protons or heavy ions–generated by an ultrahigh intensity laser, and is directed towards the pre-compressed fusion pellet. This laser generated particle beam is supposed to deliver sufficient energy locally to ignite the fusion-fuel and to start a burn wave. The ignition conditions in the fast ignitor scenario have been discussed and studied in detail previously [4–8], here we discuss the properties of beam transport and energy deposition of high intensity charged particle beams.

Since the discovery of alpha decay and the availability of energetic fission fragments, it became interesting to study fast particle stopping processes in matter [9–11]. In past decades experimental investigation of the stopping power of ionized matter became possible and sparked numerous efforts to describe single particle stopping in plasma and warm dense matter [12–19]. A number of theoretical approaches which may considered further developments of the early work of Bethe [16] and Bloch [17] do treat the energy loss of ions in ionized matter. But only recently experiments with sufficient precision were carried out to distinguish between different models [20, 21]. Mono-energetic particles generated from laser induced nuclear reactions [20] or the UNILAC accelerator at GSI [21] were used. In both experimental approaches the beam intensity was low enough to test the model of single particles interacting with high temperature dense plasma. The beam particle density was orders of magnitude lower than the plasma density and thus the inter-particle distance of the beam is much larger than the plasma screening length. Previous experiments with laser generated particle beams [22, 23] have demonstrated intense beam density (10^{19} cm^{-3}) and short pulse duration (pico-second). Thus particle beams generated from ultrahigh-intensity lasers open a new realm, where beam-driven complex collective phenomena are expected to occur [24–30], resulting in anomalous stopping. In order to improve our understanding of these effects, experimental data are required.

In this Letter, we report about a key experiment to study the effect of anomalous stopping induced by high intensity laser-accelerated proton beams in dense ionized matter. A magnetic dipole was used to tailor a short and quasi-mono-energetic proton beam of 3.4 MeV with an energy spread of 6%. The target of dense ionized matter was produced from irradiating a carbon-hydrogen-oxygen foam sample (TAC) with soft x-rays from a laser-heated hohlraum. The hydrodynamic timescale of the target is long compared to the short proton beam pulse and

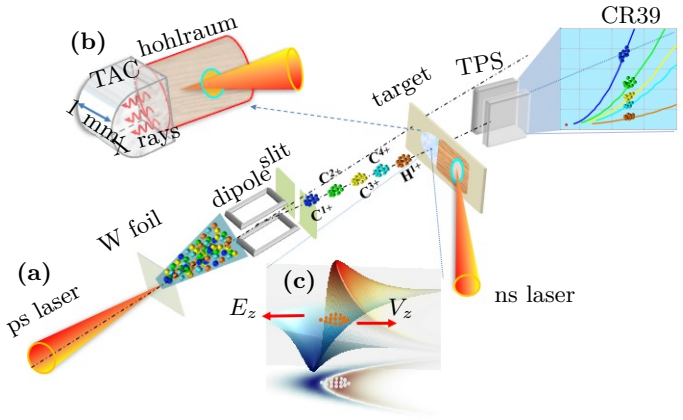

FIG. 1. (a) A ps laser is focused onto a Carbon-coated tungsten foil, generating intense short-pulse ion beams with different species. A magnetic dipole and a limiting slit serve as $\mathbf{p}/q$ analyser to select mono-energetic ion beams. Such ions interact with the laser generated plasma-target and emerge from the target with a lower energy due to the incurred energy loss. The final-state energy is measured by a Thomson parabola in conjunction with CR39 film. (b) The target consists of a gold hohlraum converter to produce the soft x-rays that irradiate the TAC foam to generate a dense ionized sample. (c) The insert shows the simulation result of an intense proton beam moving along the z direction, inducing a strong longitudinal electric field, which is counter directional to the proton beam propagation, causing anomalous stopping.

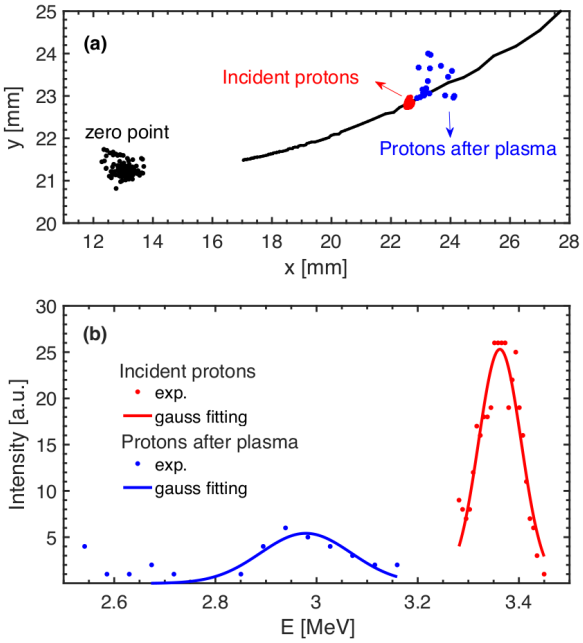

FIG. 2. (a) Tracks of protons recorded on TPS CR39 passing through null target and plasma target. The X and Y coordinates represent the magnetic and electric deflection distances. The dashed curve represents the deflected position for various proton energies. The tracks for the zero reference point as well as the protons with/without plasma are indicated with black, blue and red dots respectively. (b) Energy spectra of the protons passing through null target and plasma target.

therefore the target can be considered to be quasi static with well characterized plasma parameters of 17 eV electron temperature and an electron number density of 4×10^{20} cm^{-3}. We observed enhanced stopping properties by one order of magnitude as compared to the classical single particle stopping in cold matter. We attribute this phenomenon to a strong decelerating electric field with a maximum on the order of 10^9 V/m, which is induced by the intense proton beam. Our numerical simulation shows that this collective effect plays the dominant role, and it will have major impact on nuclear fusion scenarios like fast ignition, but also for applications in material science and astrophysics.

Experiment was carried out on XG-III laser facility at Laser Fusion Research Center with the experimental layout displayed in Fig. 1. Here a short and intense laser beam with duration 800 fs and energy 150 J is focused on a tungsten foil [70 μm of transverse size and 15 μm-thick]. Intense ion beams, containing protons (H^{1+}) and C-ions with different charge states (C^{1+}, C^{2+}, C^{3+} and C^{4+}), are produced on the backside through the mechanism of target normal sheath acceleration (TNSA). Among such particle species, proton (H^{1+}) is proven to be the dominant one [22, 23], as its charge to mass ratio is the highest and experiences a higher acceleration efficiency than other carbon ions. As ion energy spectra through TNSA are usually broad, in order to reduce the bandwidth of ion spectra, here a magnetic dipole, as shown in Fig. 1(a), was used to tailor the broad spectra and select a short and quasi-mono-energetic proton beam. The magnetic field of dipole is 0.8 Tesla and thickness of slit is 500 μm. They served as a $\mathbf{p}/q$ analyser, where $\mathbf{p}$ and q are the particle momentum and charge respectively. Thus particles with small $\mathbf{p}/q$ have the highest deflection, and quasi-mono-energetic ions are therefore selected. Please note although the selected ions still contains different species, each has different velocity and would research the plasma target independently with different time delay.

As for the target, a gold hohlraum converter was used to produce soft x-rays by the interaction of a ns laser [energy of 150 J] with the wall of the gold hohlraum, irradiating the TAC foam [density of 2 mg/cm^{-3} and thickness of 1 mm], and producing dense ionized plasmas therein. Due to the deep penetration of soft x-rays, the foam was heated quasi isochronally. Existing work had demonstrated the specific hydrodynamic response of this x-ray heated foam [31–33]. The hydrodynamic timescale of the target is long (ns-living) compared to the short proton beam pulse and therefore the target can be considered to be quasi static with well characterized plasma conditions. In order to determine plasma conditions, emission spectra from gold hohlraum and TAC matter were measured. Gold hohlraum radiation fits well with

20 eV black body spectra, and the electron temperature of foam plasma was determined to be around 17 eV when analysing the intensity profile of helium-like carbon lines by using Boltzmann curve slope method. Under local thermodynamic equilibrium conditions, according to calculations of FLYCHK code [34, 35], the ionization degree of TAC matter is $C_{12}^{3.7+}H_{16}^{0.99+}O_{8}^{4.4+}$, under which the free electron density is 4×10^{21} cm^{-3}.

In order to diagnose the energy spectra of charged protons, a Thompson parabola spectrometer (TPS) in conjunction with a plastic track detector CR39 was taken. On TPS device, a pinhole with radius of 200 μ m was opened, which enable this device to achieve energy resolution of $\delta E = 0.07$ MeV for 3.36 MeV protons. In Fig. 2(a), tracks recorded on CR39 for protons passing through null target and plasma target as well as the zero reference point are displayed. Based on the magnetic deflection distance, proton kinetic energy value was analysed. As we can see in Fig. 2(b), the energy spectra for incident protons with a 3.36 MeV peak energy and full width at half maximum (FWHM) 0.06 MeV, are significantly downshifted, for which the peak energy was decreased to 2.98 MeV and FWHM was increased to 0.2 MeV after passing through plasmas. The measured energy loss in experiment is compared with theoretical predictions as shown in Fig. 3. For existing theoretical models, for example Bethe-Bloch model, Li-Petrasso (LP) theory [12] and Standard Stopping Model (SSM) by Deutsch [13], which account for only collisions of an individual proton with free electrons, bound electrons or/and plasmons, underestimate the stopping power, with difference as large as one order of magnitude.

We attribute this anomalous stopping to the collective electromagnetic effects induced by high current ion beams. In order to accurately and completely investigate this anomalous stopping, both collective electromagnetic effects and close particle-particle interactions need to be taken into account. PIC method in recently years has established itself as a state-of-the-art method for solving problems in kinetic plasma physics. Here, PIC simulations are performed by using a newly developed PIC code named LAPINS [36–38]. In this code, all the close interactions including proton-nuclei, proton-bound electron, proton-free electron were taken into account with a newly developed Monte Carlo binary collision model [39]. A new Monte Carlo ionization dynamics model was added as well [40], including collision ionization, electron-ion recombination and ionization potential depression. In order to simulate large scale plasmas and simultaneously avoid intractable simulation burden, instead of solving the full Maxwell's equation, a new approach that combines PIC method with a reduced model of high-density plasma based on Ohm's law was developed and benchmarked [36]. To take into account collective electromagnetic effects, the background electron inertia is neglected, and instead the background

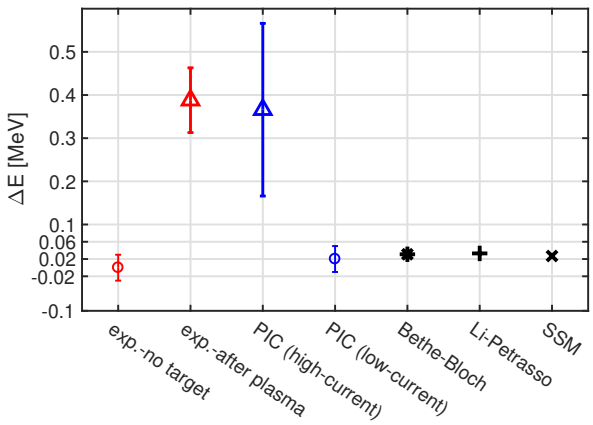

FIG. 3. Experimental, numerical (PIC) and analytical predicted energy loss of protons when passing through the dense ionized plasmas [see text for details on plasma parameters]. The experimental energy loss data (red triangle) as well as PIC simulation data (blue triangle for 8×10^7 A/cm^2 high-current case, and blue circles for 8×10^2 A/cm^2 low-current case) are evaluated as the peak energy downshift. Analytical calculations are based on Bethe-Bloch formula, Li-Petrasso theory and SSM theory. The incident energy is 3.36 MeV as shown by the red circle. The error bars for the experimental and PIC simulation data represent the FWHM of their respective energy spectra.

return current is evaluated by the Ampere's law $\mathbf{J}_e = (1/2\pi)\nabla \times \mathbf{B} - (1/2\pi)\partial\mathbf{E}/\partial t - \mathbf{J}_b - \mathbf{J}_i$, where $\mathbf{B}$ is the magnetic field, $\mathbf{E}$ is the electric field, and $\mathbf{J}_i$ is the background ion current. Applying the continuity equation $\nabla \cdot \mathbf{J} + \partial\rho/\partial t = 0$, where $\mathbf{J} = \mathbf{J}_b + \mathbf{J}_i + \mathbf{J}_e$ is the total current, Poisson Equation $\nabla \cdot \mathbf{E} = 2\pi\rho$ is rigorously satisfied. The electric fields are then solved by the Ohm's law, $\mathbf{E} = \eta\mathbf{J}_b - \mathbf{v}_e \times \mathbf{B}$, where $\mathbf{v}_e$ is the background electron velocity, and η is the resistivity. Taking advantage of the Monte Carlo collision model, resistivity η is obtained with a natural manner by averaging over all binary collisions at each time step for each simulation cell. Finally, Faraday's law is used to advance the magnetic fields $\partial\mathbf{B}/\partial t = -\nabla \times \mathbf{E}$. This field solver, which couples Ampere's law, Faraday's law and Ohm's law, can completely remove the numerical heating and significantly reduce the calculation burden. These advantageous features provide a unique tool, which can self-consistently model transport and energy deposition of intense charged particles in dense ionized matter.

In the simulation, the incident proton beam is modelled to have Gaussian distributions both temporally and spatially, with beam duration of 1 ps and transverse size of 1 mm. The energy spectra is assumed to be of Gaussian profile as well, with peak energy at 3.36 MeV spreading with FWHM of 0.06 MeV. The plasma target is parametrized the same as with that diagnosed in experiment, namely, electron temperature of 17 eV, ion-

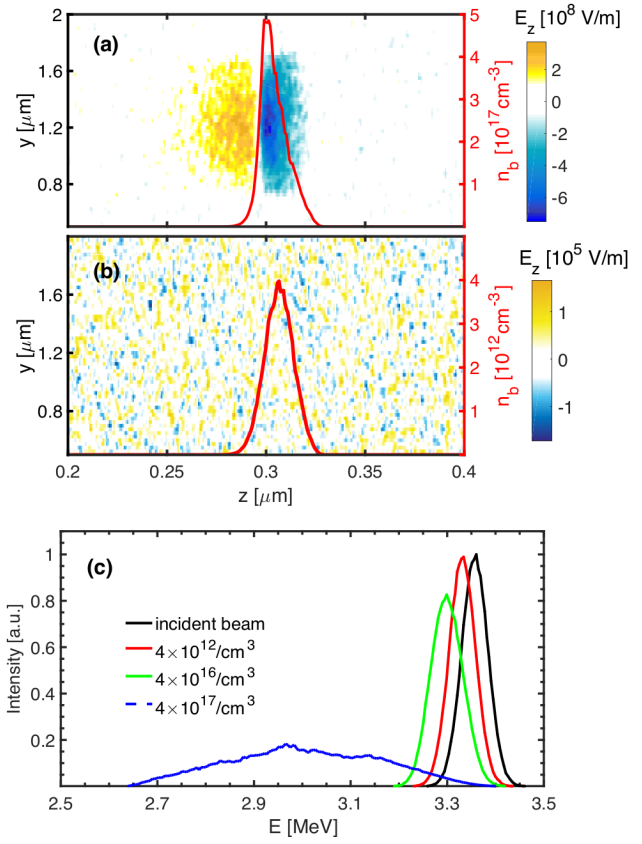

FIG. 4. (a) Longitudinal electric field driven by proton beams which moving along Z direction for the case with initial beam density 4×10^{17} cm^{-3}. The beam density profile is indicated by the red solid curve. (b) The same with (a) but the initial beam density is changed to 4×10^{12} cm^{-3}. (c) Normalized energy spectra for the incident protons (solid black curve) as well as that when passing through dense ionized plasmas. Here, different coloured lines represent cases for proton beams with different initial densities, for example, 4×10^{12} cm^{-3} by solid red curve, 4×10^{16} cm^{-3} by solid green curve, and 4×10^{17} cm^{-3} by dashed blue curve.

ization degree of $C_{12}^{3.7+}H_{16}^{0.99+}O_8^{4.4+}$, free electron density of 4×10^{21} cm^{-3}. The simulation is carried out in the Z-Y Cartesian geometry with beam propagating along Z direction. The size of the simulation box is 1.2 mm $\times$ 2.5 mm, with grid size of 0.75 μm $\times$ 25 μm, containing 25 particles per grid for each plasma species and 64 particles per grid for proton beam.

Given the incident proton beam with density 4×10^{17} cm^{-3}, peak energy 3.36 MeV, FWHM 0.06 MeV and duration 1 ps, Fig. 4(a) shows the longitudinal electric field $\mathbf{E}_z$ induced by the beam-driven return current when already propagating for 0.3 mm. Strong decelerating field $\mathbf{E}_z$ on the order of 10^9 V/m is produced, which plays the dominant role in proton stopping. The resulted energy downshift of protons after passing through 1 mm plasma is shown by dashed blue lines in Fig. 4(c). The energy distribution is significantly broadened in contrast to the initial spread. This is because, the protons in the bunch are surrounded by a decreasing decelerating field, i.e., protons with higher energies which located at the front bunch experience a smaller decelerating electric field than the ones with lower energies. Please note, the spatial size of this decelerating field is comparable to size of proton bunch, which is quite different to cases [41, 42] of plasma wake-field. The size of the latter is determined by plasma density. As we can see the peak energy of protons is shifted by 0.39 MeV, which agrees with experimental data in magnitude, and the broadening of energy spectra is also consistent with experimental observations. Therefore, PIC simulation reproduces the experimental data with initial beam density of 4×10^{17} cm^{-3} for 3.36 MeV protons, which equals to a beam current density of 8×10^7 A/cm^2, according to $\mathbf{J}_b = en_b\mathbf{v}_b$, where e is the electron charge, $\mathbf{v}_b$ is the proton velocity. When the beam current is reduced (e.g. 4×10^{12} cm^{-3}), the collisional effect plays the dominant role, in which case the PIC simulations obtain the same result as predicted by the individual proton slowing-down theories, for example Bethe-Bloch model, SSM and LP.

In order to well understand the anomalous stopping induced by beam densities, additional simulation for incident protons with density 4×10^{12} cm^{-3} and 4×10^{16} cm^{-3} were carried out. For low-current case (4×10^{12} cm^{-3}), the beam induced longitudinal electric field E_z after propagating for 0.3 mm in the plasma is shown in Fig. 4(b). When compared with the high-current case 4×10^{17} cm^{-3}, Fig. 4(a), no collective decelerating field is excited under such conditions. The proton stopping is dominated by the close particle-particle collisions. After passing through the plasma, the energy spectrum is downshifted by 0.02 MeV shown in Fig. 4(c), which agrees well with predictions of the binary-collision theory. As for the intermediate case (4×10^{16} cm^{-3}), stopping from close collision and collective electromagnetic effects are comparable with each other, under which the finial energy downshift is 0.04 MeV as shown in Fig. 4(c).

In summary, we report first experimental evidence on anomalous stopping and significantly enhanced stopping power of dense ionized matter interacting with a high-current laser-generated proton beam. A magnetic dipole was used to tailor a short and quasi-mono-energetic proton beam of 3.4 MeV with an energy spread of 6%. The target of dense ionized matter was produced from irradiating a carbon-hydrogen-oxygen foam sample with soft x-rays from a laser-heated hohlraum. The hydrodynamic timescale of the target is long compared to the short proton beam pulse and therefore the target can be considered to be quasi static with well characterized plasma parameters of 17 eV electron temperature and an electron number density of 4×10^{20} cm^{-3}. We observed enhanced stopping properties by one order of magnitude as compared to the classical single particle stopping in

cold matter. We attribute this phenomenon to a strong decelerating electric field with a maximum on the order of 10^9 V/m, which is induced by the intense proton beam. Our numerical simulation shows that this collective effect plays the dominant role, and it will have major impact on nuclear fusion scenarios like fast ignition, but also for applications in material science and astrophysics.

The work is supported by Chinese Science Challenge Project No. TZ2016005, the National Natural Science Foundation of China (Grant Numbers 11705141, 11775282, and U1532263), China Postdoctoral Science Foundation (Grant Numbers 2017M623145 and 2018M643613).

* dwu.phys@zju.edu.cn
† zhouwm@caep.cn
‡ zhaoyongtao@xjtu.edu.cn

[1] Ingo Hofmann, Matter and Radiation at Extremes 3, 1 (2018).
[2] N. G. Basov, S. Yu. Gus'kov, and L. P. Feoktistov, J. Sov. Laser Res., 13, 396 (1992).
[3] M. Tabak, J. Hammer, M. E. Glinsky, W. L. Kruer, S. C. Wilks, J. Woodworth, E. M. Campbell, M. D. Perry, R. J. Mason, Phys Plasmas 1, 1626 (1994).
[4] H. Nagatomo, T. Johzaki, T. Asahina, M. Hata, Y. Sentoku, K. Mima, H. Sakagami, Nuclear Fusion 59, 106055 (2019)
[5] N. Ratan, N. J. Sircombe, L. Ceurvorst, J. Sadler, M. F. Kasim, J. Holloway, M. C. Levy, R. Trines, R. Bingham, P. A. Norreys, Physical Review E 95, 013211 (2017).
[6] T. Yanagawa, H. Sakagami, A. Sunahara, H. Nagatomo, Laser and Particle Beams 33, 367 (2015).
[7] M Temporal, R Ramis, B Canaud, V Brandon, S Laffite, B J Le Garrec, Plasma Physics and Controlled Fusion 53, 124008 (2011).
[8] M Temporal, R Ramis, J J Honrubia, S Atzeni, Plasma Physics and Controlled Fusion 51, 035010 (2009).
[9] D. H. H. Hoffmann, V. E. Fortov, I. V. Lomonosov, V. Mintsev, N. A. Tahir, D. Varentsov, and J. Wieser, Phys. Plasmas 9, 351 (2002).
[10] V. Mintsev, V. Kim, I. Lomonosov, D. Nikolaev, A. Ostrik, N. Shilkin, A. Shutov, V. Ternovoi, D. Yuriev, V. Fortov, A. Golubev, A. Kantsyrev, D. Varentsov, and D.H.H. Hoffmann, Contrib. Plasma Phys. 56, 281 (2016).
[11] J. Ren, C. Maurer, P. Katrik, P.M. Lang, A.A. Golubev, V. Mintsev, Y. Zhao and D.H.H. Hoffmann, Contributions to Plasma Physics, 58, 82 (2017).
[12] C.-K. Li and R. D. Petrasso, Phys. Rev. Lett. 70, 3059 (1993).
[13] C. Deutsch, G. Maynard, M. Chabot, D. Gardes, S. Della-Negra, R. Bimbot, M.-F. Rivet, C. Fleurier, C. Couillaud, D. H. Hoffmann, et al., The open plasma physics journal 3 (2010).
[14] G. Maynard and C. Deutsch, Journal de Physique 46, 1113 (1985).
[15] W. Cayzac, V. Bagnoud, M. M. Basko, A. Blazevi, A. Frank, D. O. Gericke, L. Hallo, G. Malka, A. Ortner, A. Tauschwitz, J. Vorberger, and M. Roth, Phys. Rev. E 92, 053109 (2015).
[16] H. Bethe, Annalen der Physik 397, 325 (1930).
[17] F. Bloch, Annalen der Physik 408, 285 (1933)
[18] L. S. Brown, D. L. Preston, and R. L. Singleton, Physics Reports 410, 237 (2005).
[19] D. O. Gericke, Laser and Particle Beams 20, 471 (2002).
[20] A. B. Zylstra, J. A. Frenje, P. E. Grabowski, C. K. Li, G. W. Collins, P. Fitzsimmons, S. Glenzer, F. Graziani, S. B. Hansen, S. X. Hu, M. G. Johnson, P. Keiter, H. Reynolds, J. R. Rygg, F. H. Seguin, and R. D. Petrasso, Phys. Rev. Lett. 114, 215002 (2015).
[21] W. Cayzac, A. Frank, A. Ortner, et al Nat. Commun. 8, 15693 (2017).
[22] T. Bartal, M. E. Foord, C. Bellei, M. H. Key, K. A. Flippo, S. A. Gaillard, D. T. Offermann, P. K. Patel, L. C. Jarrott, D. P. Higginson, et al., Nature Physics 8, 139 (2012).
[23] B. M. Hegelich, B. Albright, J. Cobble, K. Flippo, S. Letzring, M. Paffett, H. Ruhl, J. Schreiber, R. Schulze, and J. Fernandez, Nature 439, 441 (2006)
[24] J. Kim, B. Qiao, C. McGuffey, M. Wei, P. Grabowski, and F. Beg, Physical review letters 115, 054801 (2015).
[25] S. Chen, S. Atzeni, T. Gangolf, M. Gauthier, D. Higginson, R. Hua, J. Kim, F. Mangia, C. McGuffey, J.-R. Marques, et al., Scientific reports 8, 14586 (2018).
[26] C. Deutsch and G. Maynard, Matter and Radiation at Extremes 1, 277 (2018).
[27] S.-w. Chou, J. Xu, K. Khrennikov, D. E. Cardenas, J. Wenz, M. Heigoldt, L. Hofmann, L. Veisz, S. Karsch, et al., Physical review letters 117, 144801 (2016)
[28] M. Honda, J. Meyer-ter Vehn, and A. Pukhov, Phys. Rev. Lett. 85, 2128 (2000).
[29] M. Tatarakis, F. N. Beg, E. L. Clark, A. E. Dangor, et al Phys. Rev. Lett. 90, 175001 (2003).
[30] B. Vauzour, A. Debayle, X. Vaisseau, S. Hulin, H.-P. Schlenvoigt, D. Batani, S. Baton, J. Honrubia, P. Nicolai, F. Beg, et al., Physics of Plasmas 21, 033101 (2014).
[31] O. Rosmej, et al Nuclear Instruments and Methods in Physics Research Section A: Accelerators, Spectrometers, Detectors and Associated Equipment 653, 52 (2011).
[32] O. Rosmej, N. Suslov, D. Martsovenko, G. Vergunova, N. Borisenko, N. Orlov, T. Rienecker, D. Klir, K. Rezack, A. Orekhov, et al., Plasma Physics and Controlled Fusion 57, 094001 (2015).
[33] S. Faik, A. Tauschwitz, M. M. Basko, J. A. Maruhn, O. Rosmej, T. Rienecker, V. G. Novikov, and A. S. Grushin, High energy density physics 10, 47 (2014).
[34] H. K. Chung, M. H. Chen, W. L. Morgan, Y. Ralchenko, and R. W. Lee, High Energy Density Physics 1, 3 (2005).
[35] Refer to https://www-amdis.iaea.org/FLYCHK/ for online computing
[36] D. Wu, W. Yu, Y. T. Zhao, D. H. H. Hoffmann, S. Fritzsche, and X. T. He, Phys. Rev. E 100, 013208 (2019).
[37] D. Wu, W. Yu, S. Fritzsche, and X. T. He, Phys. Rev. E 100, 013207 (2019).
[38] D. Wu, X. T. He, W. Yu, and S. Fritzsche, High Power Laser Sci. Eng. 6, e50 (2018).
[39] D. Wu, X. T. He, W. Yu, and S. Fritzsche, Phys. Rev. E 95, 023208 (2017).
[40] D. Wu, X. T. He, W. Yu, and S. Fritzsche, Phys. Rev. E 95, 023207 (2017).
[41] C. Huang, W. Lu, M. Zhou, C. E. Clayton, C. Joshi, W. B. Mori, et al Phys. Rev. Lett. 99, 255001 (2007).
[42] P. Muggli and the AWAKE Collaboration, Plasma Phys. Control. Fusion 60, 014046 (2018).